

Characterization of a MRI-RF Hyperthermia Dual-Function Coil Element Design

X. Yang¹, J. Wu², X. Chu¹, T. K. Foo³, and D. Yeo³

¹Power Conversion Circuits Lab, GE Global Research, Shanghai, China, People's Republic of, ²Electrical and Computer Engineering, Northeastern University, Boston, MA, United States, ³Imaging Technologies, GE Global Research, Niskayuna, NY, United States

INTRODUCTION: During a mild RF hyperthermia procedure for cancer treatment, careful monitoring of intratumoral and surrounding healthy tissue temperature is required [1]. Existing systems typically use a separate coil for heating and the MR scanner's RF birdcage body coil for MR thermometry, which has led to image artifacts due to cross-talk, oscillations [2] and low SNR [3]. The use of the same physical coil for MRI and heating will significantly mitigate these artifacts and thus enable more accurate MR thermometry images. In this study, EM simulations-based analyses of a proposed dual-function coil element are performed. The element has the potential to transform between heating and MR imaging modes in real-time via the use of fast RF switches. Such a dual-function array will be closer to the body, thus potentially increasing SNR and acquisition speed (via parallel imaging) of MR thermometry.

METHOD: The proposed dual-function coil element is based on a MR loop coil layout that transforms into a C-shaped dipole antenna for heating (Fig 1). Mode switching is achieved in a dual-function element by adding (for imaging) or removing (for heating) two capacitors in real-time – a loop capacitor opposite the drive port and an impedance matching capacitor at the drive port. Figure 2 shows a proposed switching control circuit for two coil elements, which are controlled by external DC control signals A and B. Axially polarized dipole antenna arrays have been shown to be capable of 3D focusing and steering of RF energy in a subject [4] and MR loop coil arrays are commonly used for MRI. Following the analyses in [5], the current distribution of a C-typed dipole antenna of length $2a$ with wire radius a_0 is

$$\vec{J}(\vec{r}) = \frac{I}{2\pi a_0} \left\{ \begin{array}{l} \hat{z} \left(1 - \frac{|z|}{4a}\right) \quad |z| \leq a, x = 0 \\ \pm \hat{x} \left(1 - \frac{x+a}{4a}\right) \quad 0 \leq x \leq 2a, |z| = a \\ -\hat{x} \left(1 - \frac{4a-x}{4a}\right) \quad |z| \leq a, x = 2a \end{array} \right\}$$

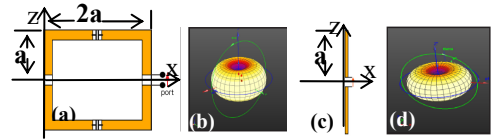


Fig. 1. (a) C-typed dipole and (b) its radiation pattern. (c) straight dipole antenna and (d) its radiation pattern.

where \hat{z} is the z-direction unit vector. Compared with a straight dipole antenna's current distribution, i.e., $J(r) = \hat{z}(I_0/(2\pi a_0))(1 - |z|/a)$ for $-a < z < a$ [5], a C-

typed dipole antenna has a higher and more homogenous current distribution, and the extended copper strips add to the effective antenna length, making it closer to half a wavelength at 127.74MHz. The matching can be improved by decreasing the capacitive reactance and potentially allowing for higher RF radiation efficiency. Furthermore, the C-type dipole antenna's radiation pattern is similar to a straight dipole's, which provides the possibility of steering the RF energy in an applicator consisting of C-type antennas. 3-D SAR steering was verified with EM simulations (SEMCAD, Zurich, Switzerland), when drove the C-typed dual-function applicator with optimized phases and amplitudes. Trade-off investigations between MR imaging and RF hyperthermia have been done with EM simulations considering these parameters: layer-to-layer overlap area, inter-element coupling, outer dimension of coils. For this study, a circular muscle phantom ($\epsilon = 63.495$, $\sigma = 0.72$ S/m, $\rho = 1040$ kg/m³) was used to simulate the body model. The length and diameter are 40 and 21.5cm, respectively. A 5cm thick water bolus ($\epsilon = 76.5$, $\sigma = 0.0001$ S/m) was placed around the phantom for energy coupling. Twenty-four loop-to-C-shaped dipole antennas (length of side=10.5cm) were symmetrically distributed on the outer surface of the water bolus in 3 rings (Fig.3).

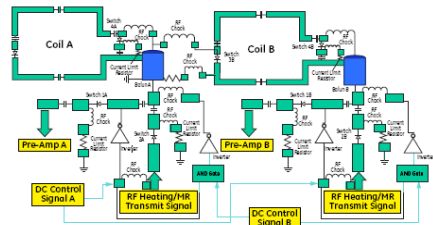


Fig. 2. Switching circuit of dual-function applicator (2-element example).

simulations (SEMCAD, SPEAG, Zurich, Switzerland), when drove the C-typed dual-function applicator with optimized phases and amplitudes. Trade-off investigations between MR imaging and RF hyperthermia have been done with EM simulations considering these parameters: layer-to-layer overlap area, inter-element coupling, outer dimension of coils. For this study, a circular muscle phantom ($\epsilon = 63.495$, $\sigma = 0.72$ S/m, $\rho = 1040$ kg/m³) was used to simulate the body model. The length and diameter are 40 and 21.5cm, respectively. A 5cm thick water bolus ($\epsilon = 76.5$, $\sigma = 0.0001$ S/m) was placed around the phantom for energy coupling. Twenty-four loop-to-C-shaped dipole antennas (length of side=10.5cm) were symmetrically distributed on the outer surface of the water bolus in 3 rings (Fig.3).

RESULTS AND DISCUSSION: Since overlap is often necessary in MR loop coil arrays for adjacent coil element decoupling, we investigate how such overlaps will affect the heating performance of a C-typed coil array.

Fig.4a-c show three arrangements of C-shaped antennas in a single panel of the applicator: (a) under lapped (b) 0mm overlapped (c) 5mm overlapped, and (d) straight dipoles array with the similar size is used as a reference. The SAR distributions when 1W input power was delivered from each antenna's voltage source (1W, 0°) are shown in Fig.5. The overlap distances between vertically adjacent coils have negligible effects on SAR focal spot sizes, but do affect the amount of surface hotspots, especially when viewed in the coronal or sagittal plane. To investigate the inter-element coupling effect, an analysis of the 3-D SAR steering limit of the C-shaped antenna array with 5mm overlapped arrangement (Fig.4(c)) was also done. Driven with the same 1 W normalized voltage sources, the phases of the C-typed antennas along the x-direction were increased. Results show that in the middle axial slice (x-y plane) of the C-shaped antenna array (Fig.3), the SAR focal spot can be shifted up to 44mm from the phantom's center before merging with the surface hotspots. This behavior is similar to that of a similar size straight dipole array (Fig.6). In the z direction, however, the SAR focal point could only be shifted up to 50mm, which was limited compared to straight dipoles array's 65mm. A study of the coil dimensions indicate that a peak SAR up to 0.06 W/kg normalized to 1W inputs at 127.74MHz can be obtained when side lengths of the coil elements are near 10.5cm.

CONCLUSION: Several observations can be made based on the simulation results. Firstly, compared to straight dipole elements, which only have current distributed along vertical direction (z-axis), C-typed elements have both vertical (z-axis) and relatively weak horizontal currents (x-y plane). These horizontal currents will lead to worse surface hotspots, especially in some overlap cases. Secondly, although coil overlap is beneficial for MRI, it cannot decouple adjacent C-typed dipole antennas. This may limit the SAR steering extent in the z direction (Fig.3) but not in the x and y directions. Thirdly, in MRI, coil dimensions affect, among other things, the depth of available transmit and receive RF signals, and loop capacitances are necessary to keep the coil tuned. For RF hyperthermia, an antenna length of half a wavelength at the radiation frequency is preferred for maximal radiation efficiency. Preliminary heating and SAR steering experiments have been performed with a 4-element dual-function applicator using the C-shaped dipole antennas [6].

REFERENCES: [1] P. Wust, et al., Med. Phys., 28:1793, 2001. [2] Gellermann J, et al. Intl J Hyper 2008;24:327-35. [3] Stakhursky VL, et al. PhysMed Biol 2009;54:2131-2145. [4] Turner PF. Regional hyperthermia with annular phased array. IEEE Trans Biom Eng 1984;31. [5] Wen Geyi, IEEE Trans on Ant and Prop, 2003;51. [6] Yeo DTB, ISMRM 2011 (submitted).

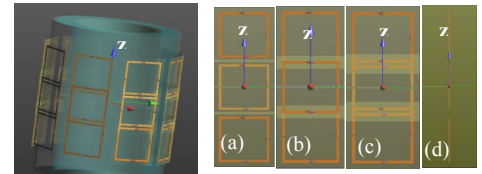


Fig. 3. Dual-function applicator with loop-to-C-shaped dipole antennas.

Fig. 4. C-shaped antennas arrangements

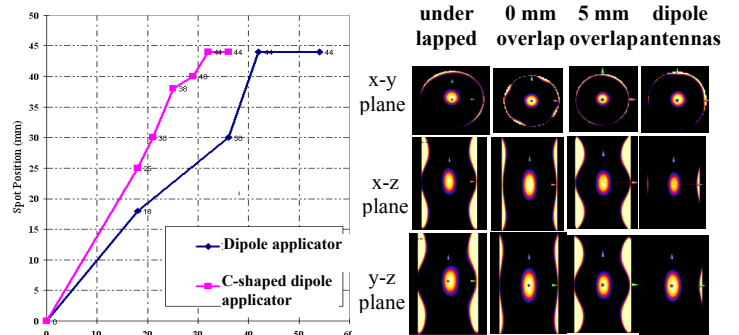


Fig. 6. Location of peak SAR in +x direction

Fig. 5. SAR distributions (middle of phantom)